IJST EXPLORE International Journal of Science and Technology
CENTRE OF PROFESSIONAL RESEARCH PUBLICATIONS
ISSN 2049-7318

International Journal of Science and Technology Volume 2 No. 6, June, 2013

Gravitational Atmospheric Tidal Potentials as Factors in Rainfall Modeling

Gachari F., Mulati D. M., Mutuku J. N.
Department of Physics. Jomo Kenyatta University of Agriculture and Technology, Nairobi, Kenya.

ABSTRACT

We present a predictive rainfall model based on fitting a Generalized Linear Model on monthly rainfall amounts with factors and covariates that determine the occurrence and persistence of the gravitational atmospheric tide state. The model demonstrates high skill while estimating monthly amounts by achieving a correlation coefficient above 0.7 between the estimates and the measurements. Model estimates of annual total for the period 1901 to 2020 indicate that the model may not only be used to estimate historical values of rainfall but also predict monthly rainfall amounts. The advantage of atmospheric tidal factors and their derivatives is that their future values are obtained accurately in advance.

Keywords: *rainfall model, atmospheric tidal potentials, rainfall projection in Kenya.*

1. INTRODUCTION

An analysis carried out by Li of time variations of the earth's length of day (LOD) versus atmospheric geopotential height fields and lunar phase showed that a strong correlation is found between LOD and geopotential height from which a close relationship is inferred and found between atmospheric circulation and the lunar cycle around the earth. It was found that there is a 27.3-day and 13.6-day east-west oscillation in the atmospheric circulation following the lunar phase change. The lunar revolution around the earth strongly influences the atmospheric circulation. During each lunar cycle around the earth there is, on average, an alternating change of 6.8-day-decrease, 6.8-day-increase, 6.8-day-decrease and 6.8-day-increase in atmospheric zonal wind, atmospheric angular momentum and LOD. The dominant factor producing such an oscillation in atmospheric circulation is the periodic change of lunar declination during the lunar revolution around the earth. The 27.3-day and 13.6-day atmospheric oscillatory phenomenon is akin to a strong atmospheric tide, which is different from the weak atmospheric tides, diurnal and semidiurnal, previously documented in the literature. Also it is different from the tides in the ocean in accordance with their frequency and date of occurrence. Estimation shows that the 27.3-day lunar forcing produces a 1–2 m s−1 change in atmospheric zonal wind. [Li, 2005]

As early as 1962, Brier and Bradley identified a 14.765 day cycle in precipitation data for the United States during the period 1871-1961 and made estimation for the lunar-solar effect on the rainfall variability by means of statistical analysis. Although no attempt was made at that time to give meteorological interpretation of the findings, they were convinced that the lunar solar effect was a significant factor in the distribution [Bradley et al, 1962], [Brier and Bradley, 1964], [Brier, 1965]. In 1995 Keeling and Whorp presented a paper proposing that extreme ocean tides may produce variation in sea surface temperatures. They proposed that dissipation of extreme tides increased vertical mixing of sea water, thereby causing episodic cooling near the surface. [Keeling and Whorp,1997].They followed the argument in 2000 by proposing that the 1800 year cycle is a possible cause of rapid climate change. [Keeling and Whorp, 2000]. Treloar in 2002 observed that lunar-solar effect produce important perturbations which he resolved into two orthogonal directions. Through time-series analysis, he found that there existed significant correlation between Southern Oscillations and sea-surface temperatures with these components. [Treloar, 2002]. In 2008 Yndestad et al used wavelet spectrum analysis to obtain correlations better than 0.7 between Atlantic water temperature cycles and the 18.6-year lunar nodal cycle. They suggested that deterministic lunar nodal tides are important regional climate indicators that should be included when future regional climate variability is considered. [Yndestad et al, 2008].

In this paper we demonstrate that monthly rainfall can be successfully modeled using factors and covariates derived from time variation of the solar-lunar geometry. We have used a Generalized Linear Model to fit monthly rainfall for the period 1951-1980 and to make a projection of monthly totals for the period 1901-2020.

2. METHODS

Climate Research Unit (CRU) of the University of East Anglia, UK, provides research datasets for the Kenya country region. We have extracted monthly total rainfall

totals for the period 1901–2000. The country aggregation is based on the CRU TS 2.0 gridded data-set. The gridded data were aggregated into countries using political boundaries according to Mitchell Hulme et al [Mitchell, T. D., et al, 2002]. The data referred to here as CRUKenya. Kenya Meteorological Department (KMD), Dogoretti Nairobi availed the rainfall data taken at Dogoretti and Jomo Kenyatta Airport stations from 1959 to 2005. The data is rain gauge measurements taken at the stations over the period and it is named KenMet data. [KenMet, 2005]. CRUKenya has been analysed and the results compared with KenMet data. National Aeronautics and Space Administration (NASA) provided solar and lunar declination values. These were obtained from ephemeris available at NASA and the values have been used to compute factors describing the relative magnitude and frequency of gravitational atmospheric tides during the period 1901 to 2050 over Nairobi. [Horizons, 2013]. The factors were then used as explanatory variables in a statistical model in which monthly rainfall is the response variable.

3. LITERATURE REVIEW

3.1 Exponetial Dispersion Model (EDM)

We assume that monthly rainfall follows one of the standard exponential dispersion family of distributions and we will therefore be an Exponential Dispersion Model (EDM). EDMs have a probability density function or a probability mass function, which can be written in the following form [Gill, 2001];

$$p(y,\theta,\varnothing,) = a(y,\varnothing)\ exp\left\{\frac{1}{\theta}[y\theta - k(\theta)]\right\} \quad (2.1)$$

where $\varnothing > 1$ is the dispersion parameter; μ is the position parameter and $\mu = k(\varnothing)$; y is the monthly rainfall amount and θ is the canonical parameter. y does not depend on the parameters θ, and $\varnothing$. The notation $y \sim ED(\mu, \varnothing)$ indicates that a random variable y comes from the EDM family, with location parameter μ and dispersion parameter $\varnothing$, as in equation (2.1). A Generalised Linear Model (GLM), satisfies two conditions: the first condition is that it is an Exponential Distribution Model in which each response variable ie $y_i \sim ED(\mu_i, \varnothing/w_i)$. The value of prior weights w_i is 1 and the second is that the expected values of the y_i, say μ_i, are related to the covariates x_i through a monotonic differentiable link function, $g(\cdot)$. The link function, $g(.)$ is the one to be determined by fitting so that

$$g(\mu_i) = \beta\, x_i^T \quad (2.2)$$

and

$$y_i = \beta\, x_i^T + e_i \quad (2.3)$$

is a linear function, hence the name –generalized linear model. and e_i are the random residues (errors in estimating y_i). [Tweedie, 1984]. In this study we use only first order factors so that $T=1$ and the Tweedie distribution of the form;

$$k(\theta) = \frac{\theta(1-p)^{(2-p)/(1-p)}}{(2-p)} for\ p \neq (1,2)$$

$$(\mu = k'(\theta), and\ variance\ function = \mu^p\ where\ \ power(p) \neq (0,1)) \quad (2.4)$$

y_i is a time series of monthly amounts from so that $y_i = y_t = y_1, y_2, y_3, ..., y_t$. Similarly, X is a TxN matrix of factors (predictors) in which each column represents a time series of each factor so that $X=x_{11}, x_{12}, ..., x_{nt}$, where $N=1,2,3, ..., n$, the number of factors and covariates. and $T=1,2,3, ..., t$. The fitting process involves obtaining values of β which linearizes the equation; $\hat{y} \approx \beta X$. $\hat{y}$ are the estimates within fit errors (residues) e_t. Hence $\hat{y}_t = \beta_0 + \beta X + e_t$. where $\beta=\beta_1, \beta_2, \beta_3, ..., \beta_n$. β_0 is the intercept and $\beta_1, \beta_2, ..., \beta_n$ are the beta values. The predictors used are described in section 2.3. It is then possible to do the matrix multiplication and obtain the time series of monthly estimates;

$$\hat{y}_t = \beta_0 + \beta_1 x_{11} + \beta_2 x_{12} + ... + \beta_n x_{nt} + e_t \quad (2.5)$$

The Tweedie Family is the family of Exponential Dispersion Models (EDMs) distributions is characterized by the power mean-variance relationship:

$$V(\mu) = \mu^p \quad (2.6)$$

as seen in (2,4).

To specify the Tweedie, the mean, μ the dispersion parameter, ϕ and the variance power, p are required. Standard algorithms are used to work out μ and Maximum Likelihood Estimate (MLE) is used to work out ϕ and p. A GLM fit on the rainfall distribution obtains the beta values used to calculate monthly rainfall estimates.

3.2 Factors

In this section we discuss how the eight predicting factors; *sdec*, *ldec*, *atide*, *etide*, *synod*, *mld*, *perigee* and *apogee* have been obtained from solar-lunar geometry. The factors are chosen because they primarily influence the gravitational excitation potential of the moon and that of the sun on the atmosphere. We consider Figure 1 where O, C and S denote the centers of the earth, moon and sun respectively and P is the point of gravitational excitation in the atmosphere close to the earth surface. OE is along the Equator. Solar and lunar declinations (*sdec* and *ldec*) are the angles EOS and EOC respectively. The angle, as measured from the equator and is positive when the target (sun or moon) is in the Northern (+) and negative in the southern (-) hemisphere.

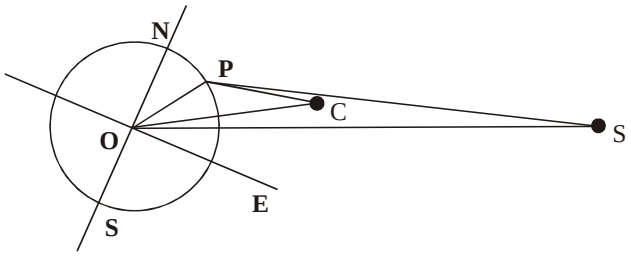

Figure 1. Geometry for calculation of tidal potentials

When we consider the tidal potential due the moon, $\Theta = \angle POC$, P is a point near the earth's surface. *N* denotes the North Pole. The potential of the attraction of *C* at point *P* is *γM/L,* where *M* denotes the mass of *C* and *γ* the gravitation constant. [Lindzen and Chapman, 1969]. The local excitation, Ω_{tidal} may be written;

$$\Omega_{tidal} = \frac{\gamma M}{(D^2 - 2aD\cos\Theta + a^2)^{1/2}} \quad (2.7)$$

where a=OP=earth radius, D=OC=earth-moon distance.

It is the acceleration at *P* relative to the earth that produces tides. The potential associated with the acceleration of the earth as a whole is

$$\frac{\gamma M}{D^2} a\cos\Theta \quad (2.8)$$

so that the excitation is maximized when Θ =0 and that P is on OC. Subtracting this from (2,8 above) we get

$$\Omega_{tidal} = \frac{\gamma M}{(D^2 - 2aD\cos\Theta + a^2)^{1/2}} - \frac{\gamma M}{D^2} a\cos\Theta \quad (2.9)$$

Expanding (2,9) in powers of *(a/D)*, and retaining only the first term, we get

$$\Omega_{tidal} \approx -\frac{3}{2}\frac{\gamma M a^2}{D^3}\left(\frac{1}{3} - \cos^2\Theta\right) \quad (2.10)$$

An equivalent equation for the solar gravitation excitation is obtained by replacing the value of *M* by the mass of the sun. Thus the excitation is inversely proportional to the cube of the lunar or solar distance and is maximum when $\Theta = 0$.

In this study an atmospheric tide state, *atide* occurs whenever O, C and S are co-linear or nearly collinear. O C and S were taken to be nearly collinear if the magnitude of the difference between *sdec* and *ldec* is less than 2 degrees. At that time the atmospheric tide is present somewhere in the tropics and not necessarily at P. An enhanced tide (etide) was taken to occur when points OPCS are co-linear. During that time, the enhanced tide is now located at P and *sdec*=latitude at P (overhead moon and sun at P). Etide occurs only during the new moon phase. We notice that a solar eclipse event condition at P is satisfied whenever PCS are co-linear but that will not necessarily satisfy either the *atide* or the *etide* state at P. Thus the solar eclipse will always have tidal effects at some location where the declinations coincide with the latitude. See Figure 2.

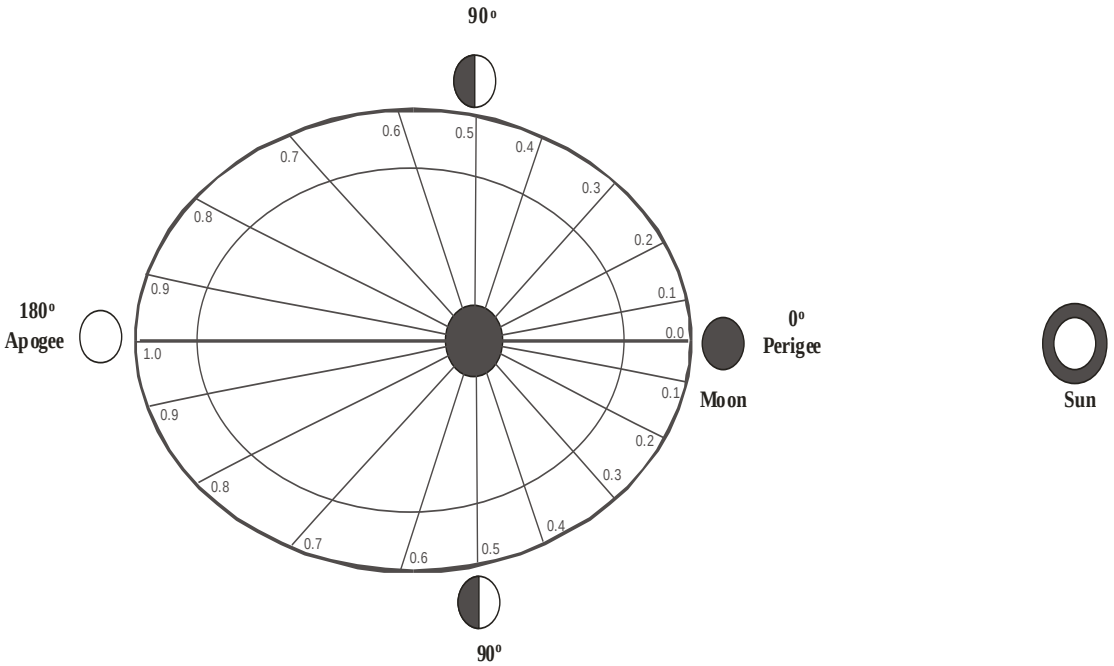

Figure 2. Lunar orbit showing New moon at perigee, the condition for the greatest tidal forces

Due to the elliptic nature of the lunar orbit the relative strength of the tidal force within a lunation is determined by the earth-moon distance denoted by a synodic decimal value between 0.0 and 1.0. Figure 2 shows the earth-moon system with the earth at a lunar elliptical orbit focus. The magnitude of the tidal forces are symmetrical for the two halves of the lunation. The factor representing the tidal strength in any one month was taken to be the value of the synodic decimal at mid-month and referred to as the *synod* and had a value of 1.0 at apogee and 0 at perigee.

The moon describes an orbit round the earth in a plane inclined at 5.15 º to the ecliptic; the pole of the orbit revolves about that of the ecliptic once in 18.60 years, so that the inclination of the plane of the moon's orbit to the earth's equator varies between 23.45º± 5.15º or 18.30º and 28.60º.The moon's declination consequently changes during each passage round its orbit between maximum northern and southern values which may vary from 18.5º to 28.5º. The change in maximum lunar declination (*mld*) influences lunar angular velocity relative to a terrestrial observer. The value of the maximum lunar declination is the numerical value of the factor *mld* for the month. Values of *mld* used in this study for the period 1901-2050 are shown in Figure 5. MLDs have a 18.6 year cycle in agreement with Yndestad et al, [Yndestad et al, 2008].

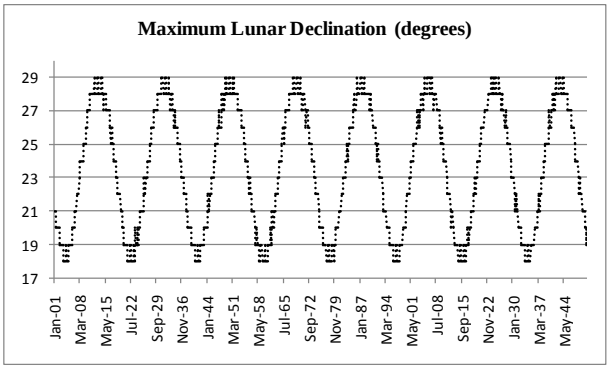

(a)

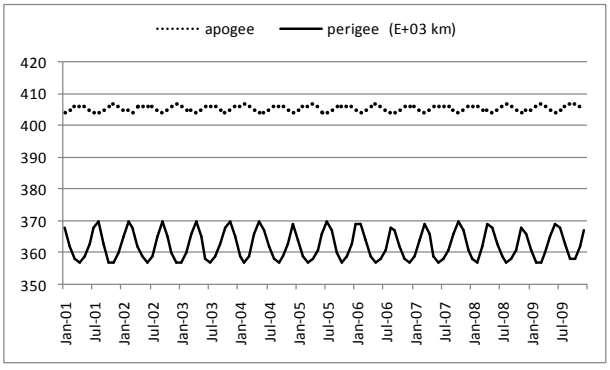

(b)

Figure 3 (a) Maximum lunar declination monthly values for the period 1901-1950 and
(b) Apogee and Perigee distances the period 1901-1910

Perigee and apogee distances vary along the lunar orbit. Mean distance of the moon from the earth is 384405 km, or 60.335 times the earth's radius (6371.2 km) while the eccentricity of the orbit is considerable, and slightly variable; the mean ratio of the maximum distance, at apogee, to the minimum value, at perigee, is 1.1162, and the maximum ratio is 1.1411. The period from one apogee to the next is called the anomalistic month and the apogee revolves round the lunar orbit once in 8.8 years as shown in Figure 3(b). For each month, the average perigee and apogee distance is calculated. Numerical values represent the factor perigee (*prg*) and apogee (*apg*) as calculated by means of a tides calculator obtained from Dcsymbols [Dcsymbols]. Figure 3(b) shows apogee and perigee distances for the period 1901-1910. We observe from equation (2,10) that perigee variation can have more significant influence on tidal variation than apogee given that tidal potential is inversely proportional to the cube of the distance. During a perigee, the moon is 40,000 km closer than during an apogee and this distance varies by about 10,000 meters twice each year. [Horizons, 2013].The lunar phase (*lunaph*) is the integral value representing any of the four lunar phases, phase one being represented by integer 1.

3.3 Proposed Design

Having discussed the method used to obtain the factors, we now discuss the rainfall model fitting procedure. This model design is based on fitting a GLM of the Tweedie family to the Nairobi rainfall on two datasets.

Model KenMet12.9 fits the KenMet dataset (1959-2003). The model is trained on the 1970-2000. The remaining segments (1959-1969 and 2001-2003) are used to validate the fit. Model CRUKenya fits the CRUKenya dataset (1901-2000). The model is trained on the 1940-1970 segments. Model validation is done using the 1901-1939 and the 1971-2000 data segments.

4. RESULTS AND DISCUSSION

Both Model CRUKenya fits the CRUKenya models fit an additive GLM of the form:

RFall~sdec+atide+ldec+mld+synod+etide+apogee+perigee.

A GLM of the Tweedie family was then fitted on both datasets and beta values obtained using a log link function. Beta values were the used to estimate monthly rainfall values for the period 1901-2020 according to equation (2.3).

Model Accuracy

For the training period, correlation between the model estimates and the measurements as well as the adjusted R-squared values are shown in Table 2.

Table 1 Goodness of fit between Model estimates and measurements

Data	Correlation Coefficients	Adjusted R^2
KenMet	0.63	0.39
CRUKenya	0.84	0.70

We observe that increasing the value of R-squared (R2) is possible by increasing the degrees of freedom within the explanatory variables but this may lead to poorer fit on test data. CRUKenya model dataset gave a better fit than KenMet model. A look at Table 1 shows a better CRUKenya fit. Moving window correlations were used to determine acuracy between the model results and the estimates over the whole of the training period. Month to month correlation obtained for each year of model training are shown in Figure 4.

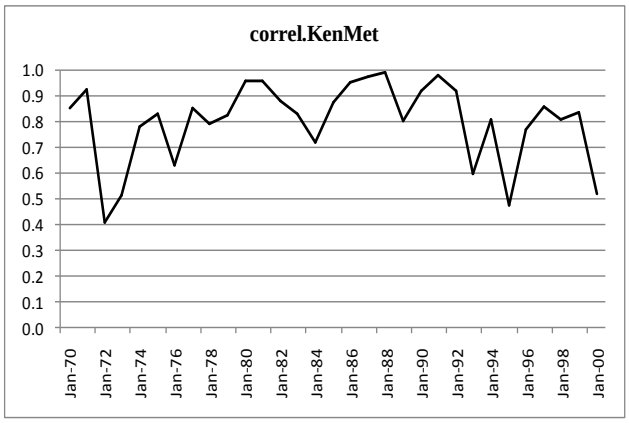

(a)

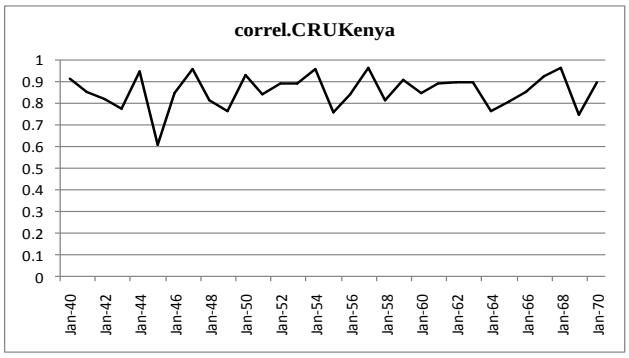

(b)

Figure 4. Moving window correlation showing month-to-month correlation for each year of model training (a)KenMet,(b)CRUKenya datasets

Models performed well during the training period with correlation above 0.4 throughout the model training period whole that of CRUKenya remained above 0.6. Models then performed projections of monthly rainfall for the periods 1959-2003 (KenMet) and 1901-2000(CRU Kenya) and a moving window correlation again used to test projection ability. as shown in Figure 5.

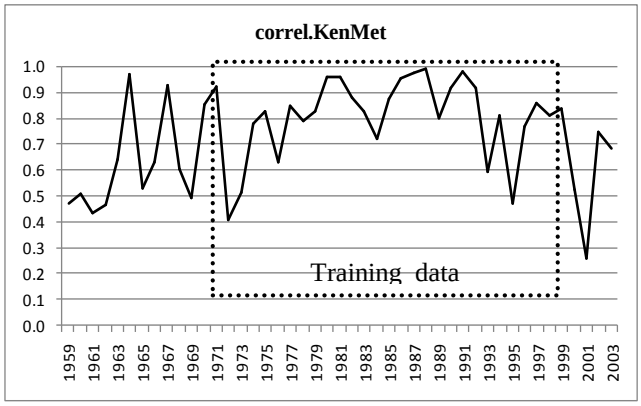

(a)

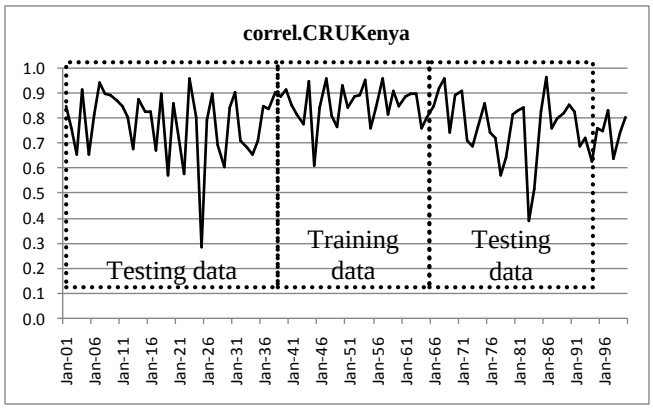

(b)

Figure 5. Moving window correlation showing month-to-month correlation for each year of model training and testing for (a) KenMet12.9 and (b) CRUKenya models

Correlation values for the training period are the ones shown in Figure 4. Projection ability is determined by the accuracy of estimates in the testing region of the dataset. Figure 5 shows no trend indicating that correlation is time dependent and that the independent is more visible in Figure 5(b). One can therefore expect a better estimate with the CRUKenya model. CRUKenya model was then used to work out monthly estimates for the period 1901-2020.Monthly estimates were then aggregated to annual values to determine inter-annual variability by standardizing values of the annual totals shown in Figure 6. Standardization was done by mean and standard deviation.Both models exhibit phase locking indicating that both models capture the same variability pattern. However, numerical summaries of the two series are different because CRUKenya is averaged for the whole country while KenMet summaries are properties of single location. See table 2

Table 3. Numerical summaries of the projected series

	mean	sd	0%	25%	50%	75%	100%	n
CRUKenya	679	79	475	623	675	730	951	120
KenMet	925	254	429	752	917	156	1980	120

KenMet12.9 and CRUKenya reliability in predicting events of severe hydrology in the country was tested against historical values. Figure 6 shows two-year averaged anomalies for the period 1901-2020 as projected by the two models; KenMet12.9 and CRUKenya.

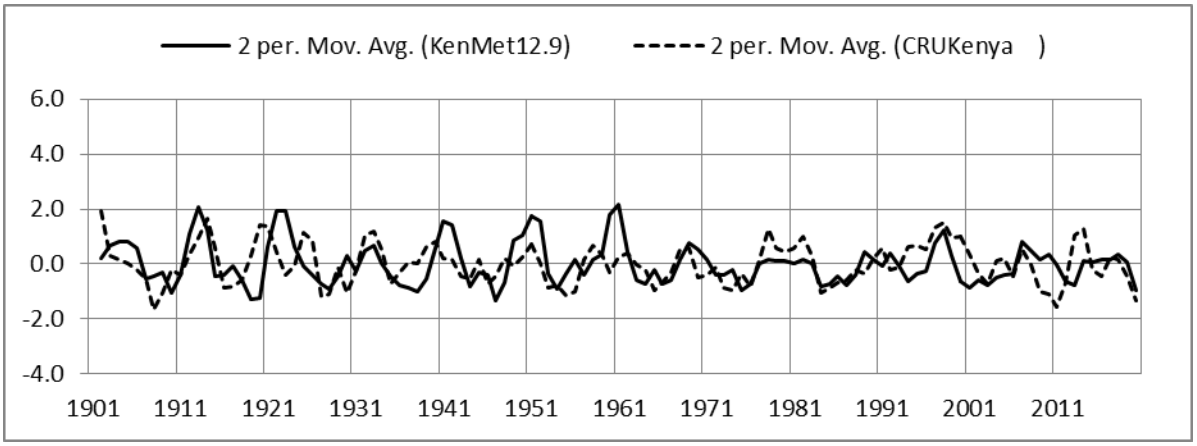

Figure 6. CRUKenya and KenMet12.9 models results showing variation of projected annual rainfall

Both models show a similar variability pattern. Model results were compared with records. Available records show periods of annual rainfall falling below normal in the following years: 1928, 1933-34, 1937, 1939, 1942-44, 1947, 1951, 1952, 1955, 1957, 1975, 1977, 1980, 1983-85, 1991-92, 1995-96, 1999-2000, 2004. [UNDP, 2004]. Others are 1960, 1965, 1969, 1973, 1976, 1987, 1993, [KenMet]. Recorded floods occurred in 1961, 1963, 1978, 1990-92, 1997-98, 2001 [KenMet]. Floods in Kenya are less devastating than droughts and therefore more interest is given to droughts. The severity of the specific drought or flood event depends on the geographical location in the country. All the droughts and floods are placed in the right years by the model.

The models estimates project above normal rainfall in 2012-2014 and below normal rainfall in 2016 and 2019-20, as seen Figure 6.

5. CONCLUSION

This study was necessitated by the need to establish the cause(s) of the Kenyan droughts of the 1984 and 2004. Two models named KenMet12.9 and CRUKenya suggest that the droughts were largely due to natural variability. This is supported by the fact that the rainfall pattern could be estimated using only solar and lunar geometry variables and their derivatives as explanatory variables in a rainfall distribution model and obtaining a correlation coefficient as higher than 0.7 between the model estimate and the measurements. It is however necessary to continue to investigate the factors which determine the unexplained variability.

Because atmospheric tidal states are the main considerations in the rainfall distribution model, there is increased likelihood that the increased severity in extreme hydrology could be related to air tides. The models indicate above normal annual rainfall in 2012-2014, and below normal rainfall in 2016, 2019-20. Further model improvements will be possible if more factors and covariates are identified which make the estimates more accurate in terms of amounts. The model may also be expanded to include multiple site estimates so long as reliable climate variables records are available for each site for a reasonably long time. Our ability to collect and store reliable data continuously will therefore always be put to test. The models have been used to predict rainfall. The same procedure may however be used on any other climate variable bearing in mind that the explanatory variables may be different for each climate variable. The statistical model successfully captured a large amount of variability in the precipitation and depicted the important relationships between the precipitation and the predictors. Considering the numerous potential sources of variability for the precipitation, the R-squared value of 0.7 obtained in the models is significant. Further work may be done in modeling of the extreme values by investigating the tail and head behaviour of the distribution with their corresponding return periods.

ACKNOWLEDGEMENTS

We wish to acknowledge the following data providers:

KMD: - Kenya Meteorological Department, Nairobi Kenya. http://www.meteo.go.ke/

NOAA:- National Aeronautics and Space Administration, Washington, DC . http://www.noaa.gov/

NASA - National Aeronautics and Space Administration. Washington, D.C. http://www.nasa.gov/

CRU: - Climate Research Unit. University of East Anglia, UK http://www.cru.uea.ac.uk/

We wish to acknowledge the following software providers:

R Foundation for the R Statistical Computing software at National Centre for Atmospheric Research (NCAR), Boulder, Colorado. August 2011. http://www.r-project.org/.

Unidata for the IDV (Integrated Data Viewer) at the Program Center, University Corporation for Atmospheric Research (UCAR), Boulder, Colorado, USA.

ConvexDNA for the Excel Mixer at rue du Nant1207 Geneva Switzerland Email info@convexdna.com

Fourmilab, for the HomePlanet at www.Fourmilab.ch. Switzerland.

REFERENCES

[1] Bradley D. A, Woodbury M. A and Brier G. W. 1962: Lunar Synodic Period and Widespread Precipitation. *Science* **137**, No. 3522, pp. 748-749.

[2] Brier G. W. 1965: Diurnal and Semidiurnal Atmospheric Tides in Relation to Precipitation Variations. Monthly Weather Review. 93, No. 2. pp. 93-100.

[3] Brier G. W. and Bradley D. A. 1964: The Lunar Synodic Period and Precipitation in the United States. Journal of the Atmospheric Sciences. 21, No. 4, pp. 386-395.

[4] Dcsymbols. 2013: Available at: http://dcsymbols.com/tides/tides2.htm

[5] Horizons, 2013. Horizons Web Interface. HORIZONS Web-Interface. http://ssd.jpl.nasa.gov/horizons.cgi?s_disp=1#top.

[6] Keeling C. D., Whorf T. P. 1997: Possible forcing of global temperature by ocean tides. Proc. Natl. Acad. Sci. 94, pp.8321-8328. Colloquium Paper.

[7] Keeling C. D., Whorp T.P .2000: The 1800-year oceanic tidal Cycle: A possible cause of rapid climate Change. PNAS. 97, No. 8. pp 3814-3819.

[8] KenMet. 2005: Kenya Meteorological Department. Data Centre. Nairobi. Available at: http://www.meteo.go.ke/.

[9] Lindzen S. R. and Chapman S. 1969: Atmospheric Tides. Space Science Reviews 10 126-128; D. ReideI Publishing Company, Dordrecht. Holland.

[10] Li Guoqing. 2005: 27.3-day and 13.6-day atmospheric tide and lunar forcing on atmospheric circulation. Advances in Atmospheric Sciences, Volume 22, Issue 3, pp 359-374.

[11] Mitchell, T.D., Hulme, M. and New, M. 2002: Climate data for political areas. Area 34, pp 109-112. Available at: http://www.cru.uea.ac.uk/~timm/.

[12] Treloar Norman C. 2002: Luni-solar tidal influences on climate variability. International Journal of Climatology. 22, pp 1527-1542.

[13] Tweedie M. C. K., 1984: An index which distinguishes between some important exponential families. Statistics - Application and New Directions, Proceedings of the Indian Statistical Institute Golden Jubilee International Conference, Indian Statistical Institute, Calcutta, pp 579–604..

[14] UNDP. 2004: Kenya Natural Disaster Profile. Enhanced Security Unit. Nairobi, Kenya.

[15] Walker, J. 2011: Fourmilab, Solar System Live. Available at: http://www.fourmilab.ch/documents/reading_list/.

[16] Yndestad Harald, Turrel William R and Ozhigin Vladimir. 2008: Lunar nodal tide effects on variability of sea level, temperature, and salinity in the Faroe-Shetland Channel and Barents Sea. Deep-Sea Research I. 55, pp 1201-1217. Available at: www.elsevier.com/locate/dsri.